Proc. Natl. Acad. Sci. USA
Vol. 93, pp. 9910–9914, September 1996
Neurobiology

Elevation of intracellular calcium by muscarinic receptor activation induces a block of voltage-activated rat *ether-à-go-go* channels in a stably transfected cell line

(K channel/modulation/293 cells)

CATHERINE E. STANSFELD*†, JOCHEN RÖPER*, JOST LUDWIG*, RÜDIGER M. WESELOH*, STEPHEN J. MARSH†, DAVID A. BROWN†, AND OLAF PONGS*‡

*Zentrum für Moleculare Neurobiologie der Universität Hamburg, Institut für Neurale Signalverarbeitung, Martinistrasse 52, D-20246 Hamburg, Germany; and †Department of Pharmacology, University College London, Gower Street, London, WC1E 6BT, England

Communicated by E. Neher, Max-Planck-Institut für Biophysikalische Chemie, Göttingen, Germany, March 29, 1996 (received for review January 15, 1996)

ABSTRACT **We have studied the properties of r-*eag* voltage-activated potassium channels in a stably transfected human embryonic kidney cell line. It was found that r-*eag* channels are rapidly and reversibly inhibited by a rise in intracellular calcium from 30 to 300 nM. The inhibition does not appear to depend on the activity of calcium-dependent kinases and phosphatases. The effect of calcium on r-*eag* channel activity was studied in inside-out membrane patches. Calcium inhibited r-*eag* channel activity with a mean IC_{50} of 67 nM. Activation of muscarinic receptors, generating calcium oscillations in the transfected cells, induced a synchronous inhibition of r-*eag* mediated outward currents. This shows that calcium can mediate r-*eag* current inhibition following muscarinic receptor activation. The data indicate that r-*eag* channels are calcium-inhibitable voltage-activated potassium channels.**

The excitability of neurons is closely linked to the activity of potassium (K) channels. These ion channels are members of evolutionarily conserved multigene families (1–3). Recently, a distinct family of K channel genes related to the *Drosophila ether-à-go-go* (*eag*) gene has emerged (4, 5). Sequence alignments of *eag* relatives from *Drosophila*, mouse, rat, and human have indicated that these K channels are structurally related both to voltage-activated K channels in the *Shaker* family and to cyclic nucleotide-gated cation channels. Heterologous expression of cloned members of the *eag* family demonstrated that the *eag* relatives express voltage-activated K channels with remarkably diverse electrophysiological properties (6–8, 22).

The *Drosophila eag* polypeptide mediated, in the *Xenopus* oocyte expression system, potassium-outward and calcium-inward currents dependent on voltage and cAMP (6). The homologous rat *eag* (r-*eag*) polypeptide gave rise to voltage-activated K channels with rather different properties in comparison to *Drosophila eag* channels and other voltage-activated K channels (7, 8). Most notably, activation kinetics of r-*eag* channels were dramatically altered by the holding membrane potential. Also, unlike *Drosophila eag* channels, r-*eag* channels did not mediate calcium-inward currents and were not modulated by cAMP. We now report that the induction of Ca^{2+} transients by the activation of muscarinic receptors was accompanied by a total transient block of r-*eag* currents in 293 cells stably transfected with r-*eag* cDNA. The Ca^{2+} inhibition was found to be rapid and reversible and was not mediated by calcineurin or Ca^{2+}-dependent kinases. In inside-out patches, we observed an exquisite Ca^{2+} sensitivity, channel activity being almost completely suppressed by cytosolic Ca^{2+} concentrations above 150 nM. These data indicate that r-*eag* channels are Ca^{2+}-inhibitable voltage-activated K channels. Thus, in neurons, they might specifically amplify excitatory stimuli related to membrane depolarization and elevation of intracellular Ca^{2+}.

MATERIALS AND METHODS

Stable Cell Lines. An *Avi*II/*Not*I fragment (nucleotides 144-3115) of r-*eag* (GenBank accession no. Z34264) in pBluescript SK^- (Stratagene) was subcloned with *Eco*RV/*Not*I into pcDNA3 (Invitrogen). 293 cells were stably transfected with pcDNA r-*eag*, using the $CaPO_4$ method (9). Of 24 clones selected, we used clone 16, which consistently gave rise to currents above 1 nA at 0 mV in whole-cell patch-clamp experiments. 293 cells stably transfected with $K_v1.1$ and $K_v1.2$ cDNA, respectively, were constructed previously using a similar protocol.

Solutions. Bath solutions contained 118 mM NaCl, 6 mM KCl, 1.5 mM $MgCl_2$, 2.5 mM $CaCl_2$, 10 mM glucose, 20 mM Hepes (pH 7.4), with NaOH. Internal solutions contained 105 mM K aspartate, 20 mM KCl, 1.5 mM $MgCl_2$, 0.5-4.1 mM $CaCl_2$, 6 mM BAPTA (acid), or 11 mM EGTA for some whole-cell experiments, 2 mM Na^{2+}-ATP, 5 mM glutathione (reduced), 10 mM Hepes (pH 7.2), with KOH. This gave free Mg^{2+} concentrations of 100 μM and free Ca^{2+} concentrations between 10 and 400 nM. For each solution, the theoretical value for free Ca^{2+} and Mg^{2+} was calculated using the program REACT V 2.01 designed by G. L. Smith (Department of Physiology, Glasgow), which calculates the equilibrium concentrations of metals and ligands in a multi-metals/multi-ligands solution. Whole-cell currents were recorded with borosilicate patch pipettes with resistances of 2–4 MΩ. For perforated patch experiments, we used a modified internal solution, containing 70 mM K_2SO_4, 10 mM KCl, 10 mM NaCl, 7 mM $MgCl_2$, 10 mM Hepes (pH 7.4), with KOH, and 0.25 mg/ml amphotericin-B (10). The perforated patches gave whole-cell access resistances of 10–15 MΩ. Chemicals were obtained from Sigma except for muscarine (Research Biochemicals, Natick, MA), indo-1 AM, ascomycin, and KN93 (Calbiochem), and cyclosporin A (a gift from Sandoz Pharmaceutical).

Electrophysiological Methods. An EPC9 (HEKA Electronics, Lambrecht, Germany) patch-clamp amplifier was used, with the programs PULSE and PULSEFIT (HEKA Electronics), for data acquisition and analysis. Leakage and capacitive currents were subtracted using the P/4 to P/8 subtraction method (the larger values for the full range current voltage

The publication costs of this article were defrayed in part by page charge payment. This article must therefore be hereby marked "*advertisement*" in accordance with 18 U.S.C. §1734 solely to indicate this fact.

Abbreviation: $[Ca^{2+}]$, Ca^{2+} concentration.

‡To whom reprint requests should be addressed.

curves). Records were digitized at 5 kHz and filtered with a low-pass Bessel filter of 1 kHz cut-off frequency. Curve-fitting for Boltzmann functions used a Sigmaplot iterative routine. Standard whole-cell experiments were performed at either 20°C or 30°C without evident difference in the observations described. Kinetics of whole-cell currents were measured at 20°C. When r-*eag* currents were activated by holding the membrane at 0 mV, 200-ms hyperpolarizing pulses to −120 mV were applied to deactivate and subsequently reactivate r-*eag* currents. The current responses were used to determine activation kinetics, specific r-*eag* current, and leak current amplitudes (Figs. 2 *B* and *C*, 5, and 6). All other experiments were performed at 20°C. Data are given as mean ± SEM, unless otherwise stated, with the number of observations in parentheses.

Patches of cell membrane were excised into a local stream of internal solution with a free [Ca^{2+}] of 30 nM. Unitary activity was recorded using an Axopatch 200 amplifier. Steady-state data was digitized and acquired on videotape. For analysis, data was filtered at 0.5 kHz, −3 dB cut-off frequency (low pass Bessel) before digitization at 2 kHz. Channel events were identified on a threshold-crossing basis set at 50% channel amplitude. At 0 mV, unitary amplitude was 0.48 ± 0.08 pA (mean ± SD), and baseline noise had an SD of 63 ± 4 fA (n = 23). Single-channel analysis used the software PAT by J. Dempster (University of Strathclyde) and SCAN by D. Colquhoun (University College London). Two-minute recordings of patches containing one or two active channels with a low open probability (0.10 ± 0.02; n = 11) were chosen for kinetic analysis. The small proportion of superimpositions (7.7 ± 1.8%) of total open time was edited out.

For the averages, PCLAMP was used for data acquisition and curve fitting, but an averaging program, QUAD (S.J.M.) was used for leak subtraction and averaging procedures. Potentials are expressed as potential deviation from ground (i.e., the inverse of that applied to the pipette). Data for Fig. 4*C* was obtained by recording steady-state activity at 0 mV for 1 min at a control 30 nM Ca^{2+}, 1 min in a test concentration of Ca^{2+} (10–300 nM), and finally recovery at the control 30 nM Ca^{2+}. The level of channel activity in each condition was expressed as overall charge transfer (current × time). Twenty-eight pairs of values were thus obtained over the range of from 10 to 300 nM calcium, and each one was normalized to the charge transfer through r-*eag* channels at 30 nM. Least-square fits of the equation $Y = Ymax/(1 + ([Ca]/K_{Ca})^n)$, were made (constrained to a common IC_{50} and Hill coefficient, but with unrestrained maxima) to each of the data pairs. Ymin was fixed at 0, and all data pairs were fitted simultaneously. The control values at 30 nM were excluded as a variable from the fit.

Spectrofluorimetry. To detect changes in cytosolic Ca^{2+}, cells were preloaded with the acetoxymethylester form of indo-1 (11) by incubation with 2 mM indo-1 AM for 30 min in culture medium at 37°C, then perfused with the external solution for 20 min to allow ester hydrolysis before beginning the experiment. Using UV epifluorescence illumination to excite indo-1, the ratio of emitted light intensities at wavelengths 407 and 488 nm was output on line to computer and digitized at 50 Hz together with the simultaneous whole-cell current record. An additional videotaped record of the current and voltage records allowed later acquisition at higher sampling rate. More detailed methods for spectrofluorimetry are described in ref. 12.

RESULTS

293 cells were stably transfected with a r-*eag* cDNA construct (r-*eag*-293 cells). Depolarization of r-*eag*-293 cells in whole-cell patch-clamp experiments evoked noninactivating r-*eag* outward currents (3.95 ± 0.31 nA at +40 mV, n = 34) (Fig. 1*A*). Their kinetic and pharmacological properties were similar to

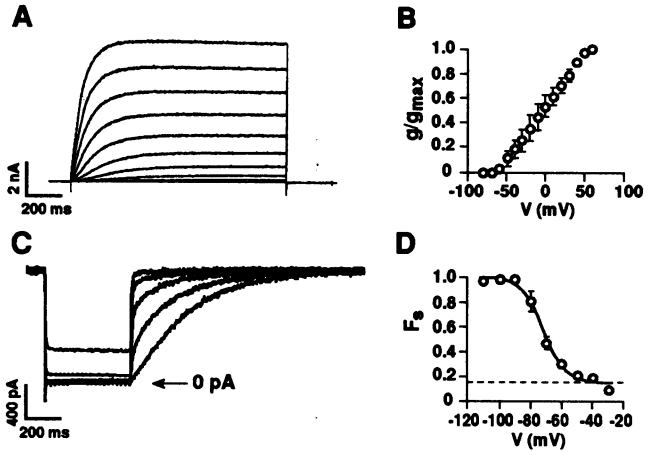

FIG. 1. Voltage-dependent activation and deactivation of r-*eag* currents in 293 cells recorded in standard whole-cell configuration. (*A*) Superimposed traces from currents evoked by 1.5-s depolarizing pulses, in 10 mV increments, to +60 mV from a holding potential of −80 mV. (*B*) Mean conductance-voltage relationship for normalized steady-state r-*eag* currents (n = 7). (*C*) From a voltage-clamp holding potential of 0 mV to activate currents, hyperpolarizing step commands of 1 s duration to between −20 and −100 mV (in 20 mV increments) were applied, returning the voltage to 0 mV. (*D*) Using the protocol shown in *C*, the current activated by stepping back to 0 mV was described by two time constants: fast (2–40 ms) and slow (100–400 ms). The fraction of the total current amplitude contributed by the slower component (F_S) was plotted against the prepulse potential (n = 4). The distribution was fit by a Boltzmann function with a half maximum at −72 mV, a slope of −7 mV and an additional steady component (15%) remaining in the slowly activating mode.

the ones previously obtained in the *Xenopus* oocyte expression system (7). The mean conductance–voltage relationship for normalized steady-state r-*eag* currents indicated a threshold for current activation of −60 mV (Fig. 1*B*). The activation curves did not show a clear saturation and, therefore, we have not attempted to describe the conductance–voltage relationship with a Boltzmann distribution. Activation kinetics strongly depended on the holding potential. As shown in Fig. 1*C*, upon stepping the membrane potential from 0 mV to hyperpolarizing potentials between −20 and −100 mV, deactivation tails were fast and not well resolved. Returning to 0 mV from the different hyperpolarizing potentials demonstrated that more hyperpolarized potentials induced very marked slowing of the kinetics of r-*eag* current activation. (Fig. 1 *C* and *D*). The kinetics could be described by two time constants indicating a fast (2–40 ms) and a slow (100–400 ms) component in r-*eag* current activation. The slow component dominated current activation, when depolarizing steps were started from more negative holding potentials. To quantify this r-*eag* characteristic behavior the slow component amplitude was expressed as a fraction of total current amplitude elicited from different prepulse potentials by depolarizing pulses to 0 mV, and the voltage range for the main transition between fast and slow kinetics was between −80 and −60 mV (Fig. 1*D*) (see also ref. 23). r-*eag* currents were relatively insensitive to 4-aminopyridine. A 30 ± 4% block (n = 6) was achieved at 50 mM 4-aminopyridine and this was voltage-independent. The IC_{50} for external tetraethylammonium block was 12 mM (n = 7). Block by quinidine was strongly voltage-dependent with little block negative to −20 mV, but an IC_{50} of 16 μM (n = 5) at +50 mV.

In standard whole-cell patch-clamp experiments with 20 nM free Ca^{2+} in the pipette solution, repeated 200-ms depolarizing pulses to +40 mV from a holding potential of −80 mV yielded stable r-*eag* current amplitudes over several minutes (Fig. 2*A*). In contrast, after establishing the standard whole-cell config-

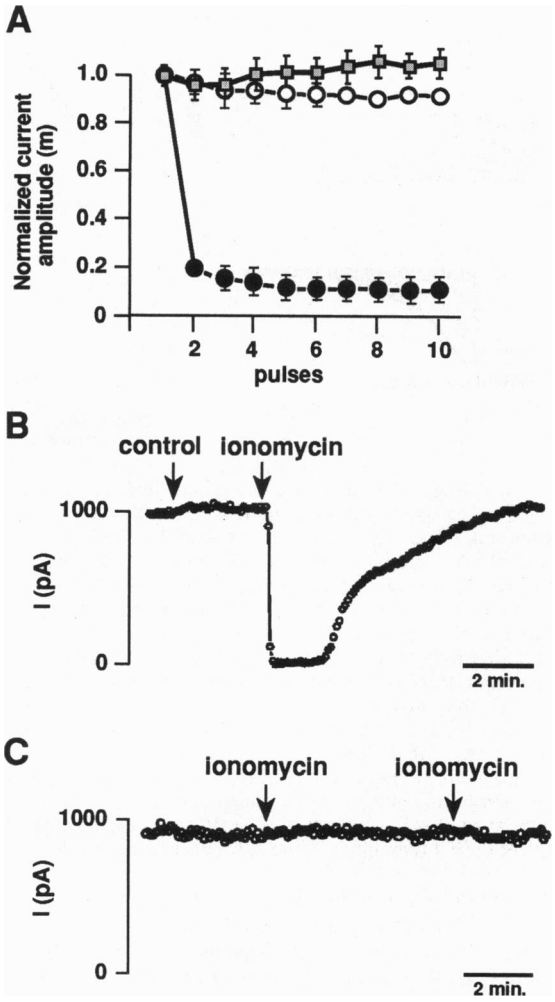

FIG. 2. Block of whole-cell r-*eag* currents by elevated intracellular Ca^{2+} concentrations. (*A*) r-*eag* (○, ●) and $K_v1.2$ (■) currents were evoked by 200-ms step depolarizations to +40 mV from a holding potential of −80 mV with 20 nM (○) (n = 5) and 400 nM (●, ▲) (n = 5) free [Ca^{2+}] in the internal solution. Normalized mean current amplitudes (m) were plotted against the number of successive depolarizations applied. Current on the first depolarizing pulse (1) was recorded shortly (20–30 s) after breakthrough into the whole-cell configuration. Subsequent pulses (2–10) were applied in 20-s intervals. (*B* and *C*) Effect of ionomycin on whole-cell current amplitudes at 0 mV for r-*eag*-293 (*B*) and $K_v1.1$-293 (*C*) cells, recorded in amphotericin-B-perforated patch configuration. Ionomycin and its solvent control (0.1% ethanol) were applied for a few seconds as indicated (arrows).

uration with an internal solution containing 400 nM free Ca^{2+}, current amplitudes dramatically declined within 2 min (Fig. 2*A*). This decline was not prevented by preincubation (>30 min) with the nonspecific protein kinase blockers H7 (50 μM) and staurosporin (1 μM) nor the CaM kinase II blocker KN93 (10 μM), nor by the calcineurin blockers cyclosporin A (1 μM) and ascomycin (10 μM). In contrast to r-*eag* currents, $K_v1.2$ current amplitudes in a stably transfected 293 cell line were not affected by 400 nM free Ca^{2+} (Fig. 2*A*) (n = 6). To maintain normal intracellular [Ca^{2+}] and buffering conditions, we used amphotericin-B-perforated patch recordings at 0 mV. Under these conditions, r-*eag* currents were essentially the same as recorded in standard whole-cell configuration at 20 nM free Ca^{2+}, except that the current density was lower [39 ± 5 pA/pF (n = 41) versus 93 ± 11 pA/pF (n = 22)], measured at 0 mV. At the same potential, nontransfected 293 cells exhibited negligible current densities (2 pA/pF, n = 10). r-*eag* currents evoked at 0 mV were completely and reversibly inhibited (Fig. 2*B*) by application of the Ca^{2+}-ionophore ionomycin (5 μM) (n = 5). The activation kinetics of r-*eag* currents measured at half-maximal recovery (47 ± 7%; n = 5) from ionomycin induced inhibition did not differ from those measured before application of the ionophore (control). Using the same protocol as in Fig. 2*B*, peak currents evoked at 0 mV from 293 cells, stably transfected with the *Shaker*-related $K_v1.1$ channels (n = 5), were not suppressed (Fig. 2*C*).

The Ca^{2+} sensitivity of r-*eag* channel activity was more directly assessed in inside-out patches excised from r-*eag* 293 cells. The channels were readily detected and could be well resolved (Fig. 1 *A* and *B*). Many patches exhibited multiple channel activity in internal solutions containing 30 nM Ca^{2+}. Like whole-cell r-*eag* currents, the channels activated at voltages positive to −60 mV and showed no inactivation but a small, partial rundown. No such channels were detected in 12 patches from control 293 cells. For unitary amplitudes measured between −60 mV and 0 mV, the mean chord conductance was 8.3 ± 0.9 pS (n = 4). Using constant-field assumptions and a permeability coefficient of 6.3 × 10^{-14} $cm^3 \cdot s^{-1}$

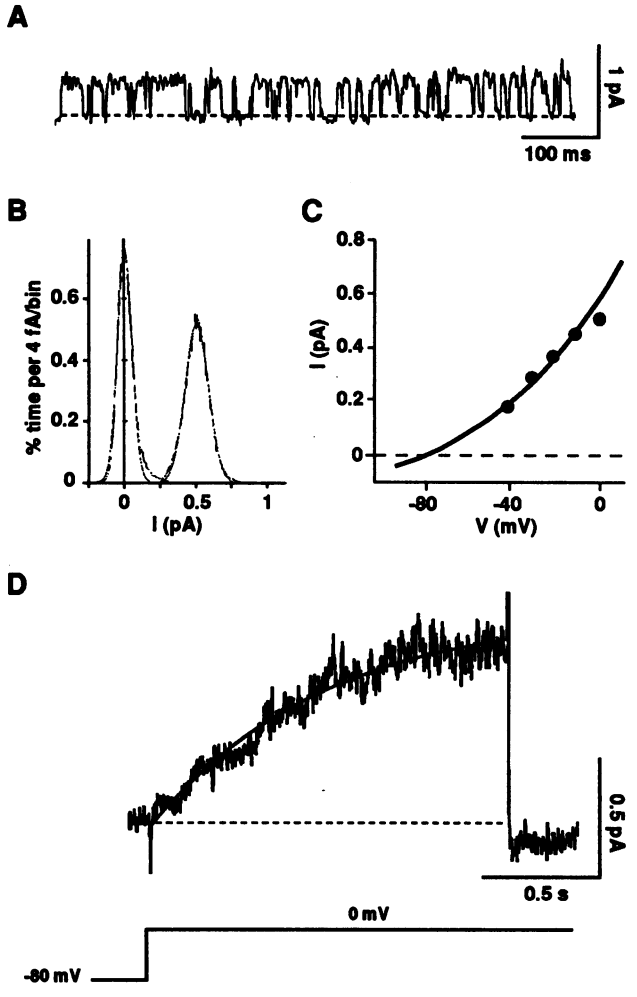

FIG. 3. r-*eag* channels in inside-out patches. (*A*) Steady-state channel activity at 0 mV (dotted line indicates the zero current level) (*B*) Amplitude histograms from the channel shown in *A* representing a 2-min record. The data were fit with Gaussian distributions with means of 0 ± 0.05 and 0.53 ± 0.08 (means ± SD) pA for closed and open channel levels, respectively. (*C*) Representative single-channel current-voltage relationship fitted, by least squares, with the Goldman–Hodgkin–Katz equation using a permeability of 4.6 × 10^{-14} $cm^3 \cdot s^{-1}$. Its conductance at 0 mV was 7.4 pS. (*D*) Ensemble current averaged from step depolarizations to 0 mV from −80 mV (n = 55). Activation was fit by a monoexponential function with a time constant of 731 ms.

(Fig. 3*C*), this corresponds to 33.5 ± 3.8 pS in symmetrical potassium. Inside-out patches were repeatedly step depolarized from −80 to 0 mV to record ensemble r-*eag* currents. They activated slowly (235–730 ms; $n = 4$) (Fig. 3*D*) similar to the slow kinetics of whole-cell r-*eag* currents (280–540 ms, $n = 5$). Channel open times at 0 mV in 30 nM Ca^{2+} had at least two components, one short and unresolved (<2 ms) and one of 7.0 ± 0.3 ms ($n = 6$).

When $[Ca^{2+}]$ in the internal solution was raised from 30 nM to 150 nM, r-*eag* channel activity was blocked by 73 ± 4.8% ($n = 6$) (Fig. 4*A*). In the suppressed state, the resolved mean open time (7.7 ± 0.5 ms; $n = 5$) and the unitary amplitude of r-*eag* channels were not changed significantly (0.52 ± 0.03 pA in 30 nM Ca^{2+} and 0.50 ± 0.03 pA in 150 nM Ca^{2+}, $n = 7$. These single-channel data imply that the mechanism underlying the Ca^{2+}-induced inhibition does not involve changes in the open state. The inhibition by Ca^{2+} was rapid and reversible (Fig. 4*B*). Ensemble r-*eag* currents averaged from single-channel recordings in response to switching the Ca^{2+} concentration from 30 to 300 nM and back to 30 nM indicated an upper limit for the time constants for inhibition and recovery of around 150 ms including the exchange times. The concentration dependence for r-*eag* channel inhibition was studied at steady state in 28 patches using different Ca^{2+} concentrations ranging from 10 to 300 nM. Data were analyzed as total charge transfer through r-*eag* channels over 1-min recording periods. Total charge transfer at different Ca^{2+} concentrations was compared with that recorded under 30 nM Ca^{2+} control conditions and normalized (see *Materials and Methods*) (Fig. 4*C*). The results indicated that channel activity was very sensitive to changes in $[Ca^{2+}]$ between 30 and 150 nM. Fitting the data yielded an IC_{50} of 67 nM for inhibition of r-*eag* channels by Ca^{2+} and a Hill coefficient of 1.5.

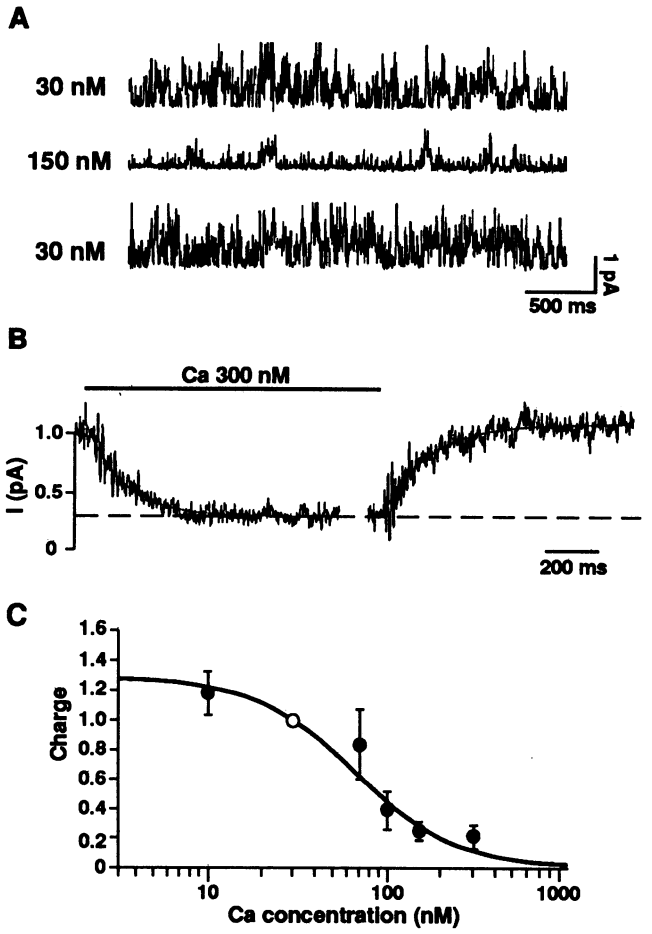

FIG. 4. Ca^{2+} block of r-*eag* channels in inside-out patches. (*A*) Steady-state channel activity at 0 mV, in the presence of internal 30 nM free $[Ca^{2+}]$, after changing to a solution with 150 nM free $[Ca^{2+}]$, and on return to 30 nM free $[Ca^{2+}]$. (*B*) Ensemble r-*eag* currents from a patch containing at least four channels, showing the response to a step increase of $[Ca^{2+}]$ in the bath from 30 to 300 nM and back, repeated 70 times for the ensemble. Current traces were fit with monoexponential functions with time constants of 131 and 175 ms, respectively. (*C*) Dose-response curve for the block of r-*eag* channel activity by $[Ca^{2+}]$ (see *Materials and Methods*). The data are represented as charge transfer normalized to their respective values at 30 nM (○, n = 28). Each solid symbol and the vertical bars represent the mean (n = 3–8) and SEM, respectively. The fitted Hill function gave an IC_{50} of 67 nM for the Ca^{2+} block.

In accordance with the high Ca^{2+} sensitivity of r-*eag* channels in excised patches, receptor-mediated induction of Ca^{2+} transients in the intact cells was accompanied by a simultaneous block of r-*eag* currents. Following activation of endogenous muscarinic receptors (13) a transient inhibition of r-*eag* current was observed, mirroring the muscarine-induced transient elevation of cytosolic Ca^{2+} (Fig. 5). These measurements were made by simultaneously recording current and fluorimetic Ca^{2+}-signals from amphotericin-B patched cells, which had been preloaded with the fluorescent dye indo-1. r-*eag* currents were measured with a holding potential at 0 mV and 200-ms hyperpolarizing steps to −120 mV repeated at 5-s intervals, to observe the activating r-*eag* currents at 0 mV. We detected no evidence of increased Ca^{2+}-entry in indo-1 preloaded r-*eag*-293 cells on activation of r-*eag* currents in the absence of muscarine. During recovery from the transient muscarinic inhibition, the activation kinetics of the partially suppressed r-*eag* currents did not appear to be altered (Fig. 5). In addition, leak conductances remained unchanged. The response of muscarine-induced fully blocked, partially blocked, and control r-*eag* currents to voltage ramps from +60 mV to −100 mV was compared. The partially blocked and control currents, when normalized, were fully superimposable (data not shown), indicating that the Ca^{2+}-induced closure of r-*eag* channels is voltage independent. About one-half of the r-*eag* 293 cells responded to muscarine. We observed 25

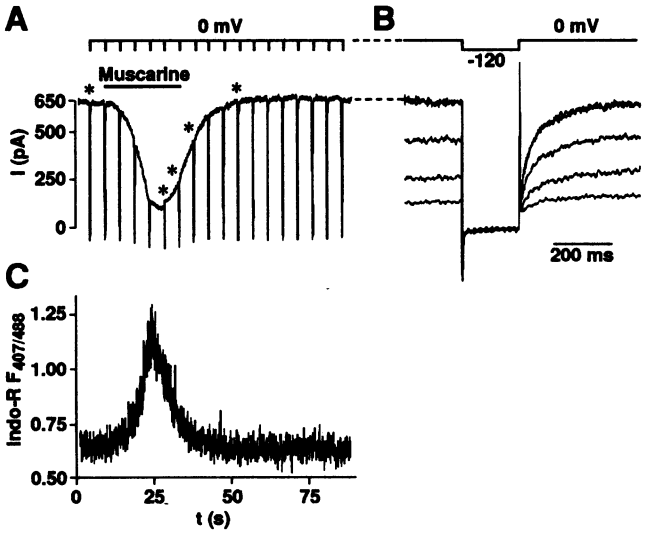

FIG. 5. Muscarinic inhibition of r-*eag* currents in 293 cells. (*A*) Whole-cell currents were activated by holding the voltage at 0 mV in the amphotericin-B-perforated patch configuration. (*B*) Asterisks in *A* mark selected current traces shown on the expanded time scale to the right. (*C*) Intracellular calcium levels were simultaneously monitored using the fluorescent indicator dye indo-1. Shown is the ratio of fluorescence detected at wavelengths 407 and 488 nm. To observe current amplitudes and kinetics, 200-ms hyperpolarizing steps to −120 mV were applied in 5-s intervals, as indicated. Muscarine (10 μM) was applied (bar).

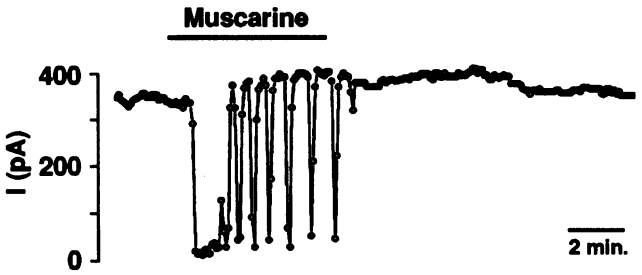

FIG. 6. Multiple fast r-*eag* current suppressions in response to muscarinic receptor activation. r-*eag*-293 current amplitudes were recorded at 0 mV in the amphotericin-B-perforated patch configuration. Muscarine (10 μM) was applied (bar).

responding cells. They exhibited either a single transient or multiple successive current suppressions (Fig. 6), each lasting approximately 8 s, with a periodicity of 45–120s. This was not regular "pacemaking," rather a self-terminating burst of spike-like phenomena (indo-1 loaded cells tended to give single-current suppressions and single Ca^{2+} transients). In similar experiments, application of 10 mM caffeine, which is known to release Ca^{2+} from ryanodine-sensitive stores in other preparations (14), induced neither a change in cytosolic [Ca^{2+}] nor a suppression of r-*eag* currents (not shown).

DISCUSSION

r-*eag* channels may represent a novel class of Ca^{2+}-inhibitable, voltage-activated K channels with the property to integrate membrane depolarization and elevation of intracellular Ca^{2+}. The exquisite sensitivity to Ca^{2+}, coupled with a low-voltage activation threshold and absence of inactivation, makes r-*eag* channels good candidates to regulate membrane excitability in rapid response to changes in intracellular [Ca^{2+}] within the lower ranges (50–200 nM) normally encountered in active neurons (15). As r-*eag* mRNA is widely expressed in rat brain, being most prominent in neocortex, hippocampal CA3 region, cerebellar granule cells, and olfactory tubercle (7), the channels could be an important component in regulation of neural excitation. Indeed, cerebellar granule cells possess a membrane current that shows some of the basic properties of r-*eag* currents, and which, like r-*eag* channels, is blocked by muscarine (16). Also, Ca^{2+} has been suggested to transduce muscarinic block of M channels (17–20). Inside-out patch experiments indicate that Ca^{2+} is unlikely to act as an open channel blocker. Although the Ca^{2+} blockade of r-*eag* channels does not appear to be mediated by Ca^{2+}-activated enzymes, it remains to be shown whether Ca^{2+} binds directly to the channels. Putative r-*eag* cytoplasmic domains are rich in acidic amino acid residues, but primary sequence analyzes did not reveal EF-hand or C_2-domain-like Ca^{2+}-binding domains.

The application of muscarine to r-*eag*-293 cells induced a transient rise and fall in intracellular Ca^{2+} concomitant with a transient suppression of r-*eag* currents. Thus, the muscarinic inhibition of r-*eag* currents, occurring within seconds, was rapid and as reversible as the Ca^{2+} inhibition of r-*eag* channel activity in excised patches. A muscarinic inhibition has also been described for *Shaker* type $K_v1.2$ channels expressed in 293 cells (21). However, in this case, channel suppression, which involved tyrosine-kinase phosphorylation, occurred in the time range of minutes. Note that $K_v1.2$ currents expressed in 293 cells were not blocked by [Ca^{2+}] elevation to 400 nM in our experimental conditions. Thus, neurotransmitter receptors may alter membrane excitability by generating different intracellular signals that suppress potassium channels either rapidly as in the case of r-*eag* channels or relatively slowly as in the case of $K_v1.2$ channels.

We are indebted to D. Colquhoun (University College London) for help with computer software and the curve fitting of Fig. 4*C*. This work was supported by grants from the Deutsche Forschungsgemeinschaft and the Wellcome Trust (to C.E.S.).

1. Chandy, K. G. & Gutman, G. A. (1994) in *CRC Handbook of Receptors and Channels*, ed. North, R. A. (CRC, Boca Raton, FL), pp. 1–71.
2. Covarrubias, M., Wei, A. & Salkoff, L. (1991) *Neuron* **7,** 763–773.
3. Jan, L. Y. & Jan, Y. N. (1994) *Nature (London)* **371,** 119–122.
4. Warmke, J. W., Drysdale, R. & Ganetzky B. (1991) *Science* **252,** 1560–1562.
5. Warmke, J. W. & Ganetzky, B. (1994) *Proc. Natl. Acad. Sci. USA* **91,** 3438–3442.
6. Brüggemann, A., Pardo, L. A., Stühmer, W. & Pongs, O. (1993) *Nature (London)* **365,** 445–448.
7. Ludwig, J., Terlau, H., Wunder, F., Brüggemann, A., Pardo, L. A., Marquardt, A., Stühmer, W. & Pongs, O. (1994) *EMBO J.* **13,** 4451–4458.
8. Trudeau, M. C., Warmke, J. W., Ganetzky, B. & Robertson, G. A. (1995) *Science* **269,** 92–95.
9. Chen, C. & Okayama, H. (1987) *Mol. Cell. Biol.* **7,** 2745–2752.
10. Rae, J., Cooper, K., Gates, P. & Watsky, M. J. (1991) *J. Neurosci. Methods* **37,** 15–26.
11. Tsien, R. Y. (1980) *Biochemistry* **19,** 2396–2404.
12. Trouslard, J., Marsh, S. J. & Brown, D. A. (1993) *J. Physiol. (London)* **468,** 53–71.
13. Choi, E. J., Wong, S. T., Hinds, T. R. & Storm, D. R. (1992) *J. Biol. Chem.* **267,** 12440–12442.
14. Furuichi, T., Kohda, K., Miyawaki, A. & Ikoshiba, K. (1994) *Curr. Opin. Neurobiol.* **4,** 294–303.
15. Miller, R. J. (1991) *Prog. Neurobiol.* **37,** 255–285.
16. Watkins, C. S. & Mathie, A. (1996) *J. Physiol. (London)* **491,** 401–412.
17. Kirkwood, A., Simmons, M. A., Mather, R. J. & Lisman, J. (1991) *Neuron* **6,** 1009–1014.
18. Selyanko, A. & Brown, D. A. (1996) *Neuron* **16,** 151–162.
19. Beech, D. J., Bernheim, L., Mathie, A. & Hille, B. (1991) *Proc. Natl. Acad. Sci. USA* **88,** 652–656.
20. Yu, S. P., O'Malley, D. M. & Adams, P. R. (1994) *J. Neurosci.* **14,** 3487–3499.
21. Huang, X. Y., Morielli, A. D. & Peralta, E. G. (1993) *Cell* **75,** 1145–1156.
22. Sanguinetti, M. C., Jiang, C., Curran, M. E. & Keating, M. T. (1995) *Cell* **81,** 299–307.
23. Terlau, H., Ludwig, J., Steffan, R., Pongs, O., Stühmer W. & Heinemann, S. (1996) *Eur. J. Physiol.* **432,** 301–312.